Istraživanja i projektovanja za privredu
ISSN 1451-4117
DOI:10.5937/jaes0-42291
www.engineeringscience.rs

iipp publishing

Journal of Applied Engineering Science
Vol. 21, No. 3, 2023
Original Scientific Paper
Paper number: 21(2023)3, 1122, 810-819

IMPROVING WEAR RESISTANCE BY ELECTROLYTE-PLASMA HARDENING OF CORROSION-RESISTANT STEEL OF THE TIP

Kuat Kombayev[1], Alina Kim[2]*, Gulden Sypainova[1], Daniyar Yelemanov[1]

[1]D. Serikbayev East Kazakhstan Technical University, 19, Serikbayeva street, Ust-Kamenogorsk, Kazakhstan
[2] Miras University, 3, Gani Ilyaeva street, Shymkent, Kazakhstan
** kim_ali@miras.edu.kz*

The development of new fields in the oil and gas industry of Kazakhstan, the exploitation of fields with hard-to-recover reserves, and the exclusion of harmful environmental impacts require the study of new advanced technologies in the manufacture of valves. Hardening of the throttle tip in the factory from low-carbon corrosion steel is provided traditionally: carburizing in a solid carburetor, followed by hardening and normalization in an electric furnace. However, this process is accompanied by high heat losses, long time spent on heating and cooling the furnace to the required temperature, and high-energy consumption - power costs are 60-100 kW/h. The carbon penetration rate is low, and for depths of 1-1.5 mm, it becomes necessary to heat the workpiece in a carburetor for 8-10 hours at a certain temperature, followed by hardening and normalization. The technological process of traditional hardening by cementation, followed by hardening and normalization, is accompanied by the appearance of various defects. The most common defects include the formation of microcracks, warpage, scale, and peeling of the metal, as well as high labor intensity and energy intensity.
A technology has been developed for hardening the tip on an electrolytic-plasma modification installation, which includes heating the part to 910-9600C and quenching in an electrolyte flow at 330-3600C, characterized in that the part is heated by electrolyte plasma, the temperature of which exceeds 6000 K. Analytically and experimentally it was determined that heating with electrolyte plasma for quenching is achieved within 4 seconds and quenching in the electrolyte flow is achieved within 8 seconds. With cyclic electrolytic plasma hardening at the 10th cycle with 40 seconds of total processing, optimal hardening rates are achieved.
An electron microscopic study of the hardened structure indicates a phase transformation and the formation of hardening martensite with a carbide network, which strengthens the steel. The tribological properties and friction coefficient of the surface layers formed during electrolytic-plasma hardening indicate an increase in the wear intensity by more than two times.

Keywords: electrolytic-plasma hardening, corrosion-resistant steel, tribological properties, stop valves, throttle

1 INTRODUCTION

When designing and manufacturing production trees in the machine-building industry of Kazakhstan, the priority is the use of rational processing modes, increasing the reliability, durability, and maintainability of equipment. The increase in manufacturability is carried out by using modern high-performance equipment and new wear-resistant materials in structures [1].

A common type of manufactured production tree is an adjustable choke. The throttle is one of the most important components of the production tree and serves as a choke device for controlling the fluid flow of the wellhead and injection valves during drilling. The throttle operates at a nominal pressure of 14 to 70 MPa and at a working medium temperature of 0 to 70 °C, Figure 1.

Adjustment of the pressure of the flow of the working medium is carried out by tip 6, the flow section of which is smoothly changed by moving the conical rod in seat 1. The movement is carried out by rotating spindle 5 on which there is a pointer showing the equivalent diameter of the flow annular section of the adjustable pressure.

In tip 6, the energy of the gas-liquid jet is absorbed and the pressure is reduced from the pressure on the buffer to the pressure in the outlet line of tee 2. The load from the tip through the split sleeve 8 is transferred to the kinematic pairs of the conical sleeve 7, the threaded sleeve 4, and the bearing cover 3. Full resource "opening and closing" of the throttle bore must be at least 1500 cycles. The “tip-seat” pair take up the entire cyclic load and abrasive wear. In the factory, highly loaded parts are heat treated with abrasion-resistant diffusion coating. It is also possible to make a throttle pair made of tungsten carbide or stellite [2].

1- Saddle assembly; 2-Tee; 3-bearing cap; 4- Threaded bushing; 5- Spindle; 6- Tip; 7- Cone bushing; 8 - Split bushing

Fig. 1. Adjustable production tree choke

In an adjustable throttle, the tip-seat pair is the most loaded. The tip is made of steel 14X17H2 (431 AISI, SAE, ASTM) of the martensitic-ferritic class is used in the hardened and normalized state. To achieve maximum strength, products made of steel 14X17H2 (431 AISI, SAE, ASTM) are subjected to hardening from 975 - 1040 ° C, exposure at a product thickness of up to 10 mm - 15 min, over 10 mm - 15 min + 1 min per 1 mm of maximum thickness, cooling - in oil. Normalization - at 275 - 350 ° C for 2 hours + 1 min per 1 mm of maximum thickness, cooling - in the air [3]. Heating of parts in the temperature range from 500 °C to 800 °C should be carried out at a rate of not more than 200 °C per hour. In the temperature range of 750 - 800 ° C, it is necessary to give an exposure until the charge is completely warmed up. Further heating to the hardening temperature is carried out according to the power of the furnace. For parts with a thickness (diameter) up to 120 mm, the heating rate is not limited and exposure at a temperature of 750 °C to 800 °C is not performed. To ensure an average level of strength after hardening, the products are subjected to tempering at 560-650 ° C for 1 hour + 1 min per 1 mm of the maximum thickness of the material, cooling in air. Heat treatment according to this mode causes the product to be prone to intergranular corrosion. To achieve high corrosion resistance, products made of steel 14Kh17N2 (431 AISI, SAE, ASTM) after hardening are subjected to tempering at 680–700 °C for 30 min + 1 min per 1 mm of the maximum thickness of the material [4]. In general, the heat treatment takes up to 20 hours in the factory, taking into account the heating and cooling of the furnace.

Traditional hardening technology requires a lot of labor, and energy costs and is not ergonomic. Therefore, research in the field of chemical-thermal treatment and subsequent introduction into production is an urgent and timely task.

2 METHODOLOGY OF EXPERIMENTAL RESEARCH

Experimental studies and mechanical tests were carried out at the VERITAS Advanced Development Center and the Mechanical Engineering Research and Production Complex of the non-profit joint-stock company of the D. Serikbayev East Kazakhstan Technical University [5].

In an adjustable throttle, the tip-seat pair is the most loaded. The tip operating in an environment of low aggressiveness is made of steel 14X17H2 GOST 5949-75 (431 AISI, SAE, ASTM), which is subject to the requirements of increased strength and hardness, table 1 [3].

Table 1. Chemical composition of the alloy 14X17H2 (431 AISI, SAE, ASTM)

C	Cr	Mn	Ni	P	S	Si
0,11-0,17	16,0-18,0	≤0,80	1,5-2,5	≤0,030	≤0,025	≤0,80

For scientific research, experimental tips were made from 14X17H2 steel (431 AISI, SAE, ASTM) from factory batches of parts, Figure 2.

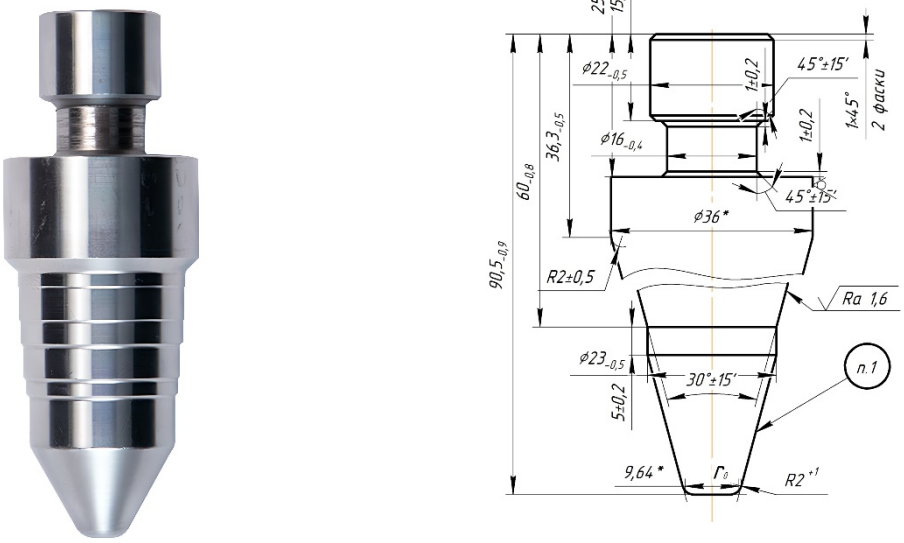

a) main view b) hardened work surface n_1

Fig. 2. Adjustable throttle tip made of steel 14X17H2 (431 AISI, SAE, ASTM)

For research, samples of microsections were cut from the tip with forming dimensions of arbitrary shape, Figure 3. After grinding, the samples were polished and etched. Polished with chromium dioxide paste. Etched with 10% ferric chloride for 3-5 seconds [6].

a) in an initial state b) after quenching EPH

Fig. 3. Preparation of a microsection from steel 14X17H2(431 AISI, SAE, ASTM)

The metallographic examination of the samples was carried out on an inverted reflected light photomicroscope "Axioscop - 2MAT" with a digital camera "Sony" [7]. The microhardness values were determined with a DuraScan-20 microhardness tester. Test method - according to Vickers, Knup. Test load - 2 kg., Exposure at maximum load - 5 seconds. Tribological tests for sliding friction were carried out on a THT-S-BE-0000 tribometer using the standard pin-disk technique (international standards ASTM G 133-95 and ASTM G 99) [8]. Tests under conditions of sliding friction according to the “pin-disk” scheme of samples made of steel 14X17H2 on a plate made of chromium-nickel austenitic steel 12X18H10T (321S31, England) were carried out without lubrication and with lubrication in tap water, at a load N = 5 H, speed v = 0.05 m /s, the run length was L = 70 m [9].

The reduced wear Ih is calculated by normalizing the test volume loss ΔV to the mileage N (m) and the applied load P (N):

$$\mathrm{Ih} = \frac{\Delta V}{NP}, \qquad (1)$$

where Ih - the reduced wear, $mm^3/(N*m)$;
N - the mileage, m;
P - the applied load, N.
A steel pin made of 100Cr6 steel with a diameter of 6 mm was used as a counter body (similar to ShKh15 steel, hardness 1550 HV, Young's modulus 220 GPa, density 7812 g/cm^3). Tests under conditions of sliding friction according to the “pin-disk” scheme of samples made of steel 14X17H2 on a plate made of chromium-nickel austenitic steel 12X18H10T (321S31, England) were carried out without lubrication and with lubrication in tap water, at a load

N = 5 H, speed v = 0.05 m /s, the run length was L = 70 m [9]. To visualize the heating process of the tip and simulate the problem of thermal conductivity when the tip is exposed to plasma energy, the software of the APM FEM strength analysis system was used.

3 RESEARCH RESULTS AND DISCUSSION

The main task in hardening a tip of a relatively small size is the determination of the temperature on the surface. Also, the low mass of the product with a complex surface determines the high sensitivity to the modes of electrolytic plasma hardening (hereinafter referred to as EPH) and the experimental determination of the optimal hardening modes. For an objective idea of the dynamics and results of the tip hardening process, a series of studies were carried out on an experimental installation for electrolytic plasma hardening. In working bath 1, a cone nozzle 4 with a built-in anode grid 7 made of stainless steel 12X18H10T (321S31), Figure 4, is installed. When a power source is connected between the cathode and the liquid electrolyte, a vapor-gas shell is formed, which is accompanied by film boiling [10]. In this short period time, the constituent components of the electrolyte are ionized and an electrolyte plasma of high temperature (more than 6000K) is excited. The tip is mounted on the clamping mechanism 6. The electrolyte circulates into the working bath through the return fitting 2. As is known, the plasma temperature significantly exceeds the temperature of the structural phase transformations, and therefore we determined the modes of electrolytic-plasma treatment experimentally. Quenching is carried out in an electrolyte flow, the best result is achieved with cyclic processing [11].

Experimentally, the heating temperature for hardening for the tip, made of steel 14X17H2 (431 AISI, SAE, ASTM), was reduced to 910-960°C, relative to traditional hardening and tempering in a furnace. At this temperature, phase transformations begin on the surface of the tip and penetrate deep into the metal during cyclic processing. Analytical study of the temperature fields of the tip during EPH allows for setting the optimal technological parameters of the electrolytic-plasma process, or correcting them taking into account the properties of materials [12].

High-speed heating from the plasma temperature is performed cyclically at regular intervals τ_{00} with a total duration of plasma treatment of one part τ_0. The interval between the plasma heating temperature intervals is assumed to be the same and equal to τ. Joule heat sources arising from the plasma temperature are concentrated in a contact spot with a diameter of $2r_0$ (diameter of the lower point of the tip cone, Figure 4) in the plane of plasma contact [13]. The heat release density of sources in x, y, z coordinates and in time is described by the Gaussian function. Heat transfer α is the sum of heat transfer from the plasma temperature (<6000 K) as a result of air convection and contact heat transfer between the tip and liquid electrolyte - 10% carbonated soda (Figure 4).

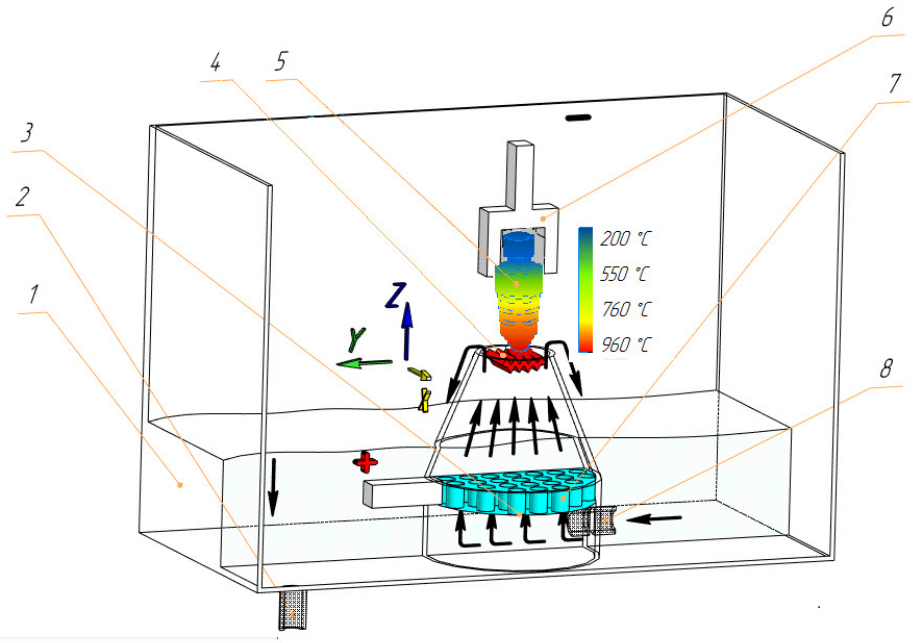

working bath, 2- electrolyte return fitting, 3-electrolyte, 4- plasma in the nozzle cone, 5-adjustable throttle tip, 6-clamping mechanism, 7- anode grid, 8- electrolyte supply fitting

Fig. 4. Model of the working bath for electrolytic-plasma hardening of the adjustable throttle tip

Under these assumptions, the differential equation of heat conduction looks like this [14]:

$$\frac{\partial T}{\partial \tau} = a\left(\frac{\partial^2 T}{\partial x^2} + \frac{\partial^2 T}{\partial y^2} + \frac{\partial^2 T}{\partial z^2}\right) + \varphi, \qquad (2)$$

where T - the temperature increment; τ - time; x,y,z - coordinates; α - the coefficient of thermal diffusivity of the workpiece material; φ-function of internal (Joule) heat sources. The function φ has the following form, given using the basic principles of the method of internal sources [15]:

$$\varphi = \frac{q_{V0}}{cp}\sum_{j=1}^{S}\exp\left[-\left(\frac{x-jt}{r_0}\right)^2-\left(\frac{y}{r_0}\right)^2-k_1\frac{z}{l_3}-\left(\frac{\tau-(j-1)\tau_{00}}{\tau_0}\right)^2\right]. \quad (3)$$

Here, q_{V0} - the heat release density at the plasma contact center at time $\tau=(j-1)\tau_{00}$; c, p - heat capacity and density of the tip material; j - the number of the plasma exposure cycle; s - the number of cycles at the EPH of the tip; k_1 - a parameter (a large positive number) that allows shifting the internal heat sources to the area of the contact spot.

The initial condition assumes zero excess temperature for the entire surface of the tip at the initial time.

Due to the small thickness of the hardened surface of the tip and insignificant heat transfer at the edges of the working zone, the boundary conditions for x and y can be considered zero [16].

Due to the symmetry and significance of heat transfer on the upper and lower surfaces of the tip, the boundary conditions for z have the form:

$$\left.\frac{\partial T}{\partial z}\right|_{z=0}=-hT;\left.\frac{\partial T}{\partial z}\right|_{z=l_3}=-hT; \quad (4)$$

Where h=α/χ— heat exchange coefficient of the flat surface of the workpiece with the environment; α- average heat transfer coefficient; χ- coefficient of thermal conductivity of the material.

Solution (2), taking into account (3) and (4), gives an expression for calculating the hardening temperature of the tip (Figure 4).

$$T = A\sum_{k,m,n=0}^{\infty}\sum_{j=1}^{S}B(k,m,n)\times\left[1+erf\left(\tau\sqrt{b_1}+\frac{b_2(k,m,n)}{2\sqrt{b_1}}\right)\right]\exp(-a\lambda^2(k,m,n)\tau)\times \quad (5)$$
$$\times\cos(b(k)x)\cos(c_1(m)y)\cos(d(n)z),$$

where

$$\begin{aligned}
&A=\frac{Q_1}{cpl_1l_2l_3};\\
&\lambda^2(k,m,n)=b^2(k)+c_1^2(m)+d^2(n);\\
&b(k)=\frac{k\pi}{(1+s)l_1};b_1=\frac{1}{\tau_0^2};c_1(m)=\frac{m\pi}{l_2};\\
&b_2(k,m,n)=-\left(\frac{2(j-1)\tau_{00}}{\tau_0^2}+a\lambda^2(k,m,n)\right);\\
&d(n)=\frac{\mu(n)}{l_3}.
\end{aligned} \quad (6)$$

In these expressions, Q_1 - the amount of heat that entered the tip during the EPH of the first section l_1; l_1, l_2, l_3– conditional areas of heating from electrolyte plasma;

$\mu(n)$ — roots of the characteristic equation corresponding to the boundary condition (4). The amount of heat Q_1, related to the heat flux density q_{V0} by the ratio [17]:

$$Q_1=\int_{-\infty V}^{+\infty}\int q_{V1}dVd\tau=q_{V0}\int_{-\infty V}^{+\infty}\int\exp\left(-\left(\frac{xt}{r_0}\right)^2-\left(\frac{y}{r_0}\right)^2-k_1\frac{z}{l_3}-\left(\frac{\tau}{\tau_0}\right)^2\right)dVd\tau, \quad (7)$$

where q_{V1} — heat release density at the EPH of the first section.

When calculating the temperature, the value of Q_1 (J) is set such that in the center of the tip the temperature is equal to or slightly higher than the temperature T of the phase transformation of the tip material. The calculated study of the temperature of the hardened tip using expression (4) was carried out with the following initial data: the material of the workpiece was steel 14X17H2 (431 AISI, SAE, ASTM), c=400 J/(kg °C),p=7800 kg/m^3, χ=32 W/(m·°C), a=1·10^{-5}

m^2/s, T= 910-960°C, l_1=0,0305 m, l_2=0,0542 m, l_3=0,0905 m, τ_{00}=4 s, τ_0=40 s, $\alpha=(\alpha_1+\alpha_2)/2$ at α_1=10 и α_2=1000 $W/(m^2 \cdot °C)$ [18].

A series of experiments determined that for heating with electrolyte plasma for quenching, the maximum heating temperature is about T_{nag}= 930-960 °C at Q_1 = 500 J at the time $\tau_1 = \tau_{00}$= 4 s.

During successive quenching in the electrolyte flow, the maximum temperature of the tip quenching in the electrolyte reaches T_{zak}= 330-360 °C. This is due to the removal of heat from the heating area of the tip due to the circulation of the electrolyte flow - 10% soda ash. The time to reach T_{zak} at the second point is equal to $\tau_2 = \tau_{00}+\tau_1$=8 s. By this moment, the temperature of the tip decreases because of the thermal conductivity of the electrolyte and heat transfer to the environment [19].

Cyclic electrolytic plasma heating leads to an even greater increase in the maximum temperature of the tip and a decrease in temperature by electrolyte flows.

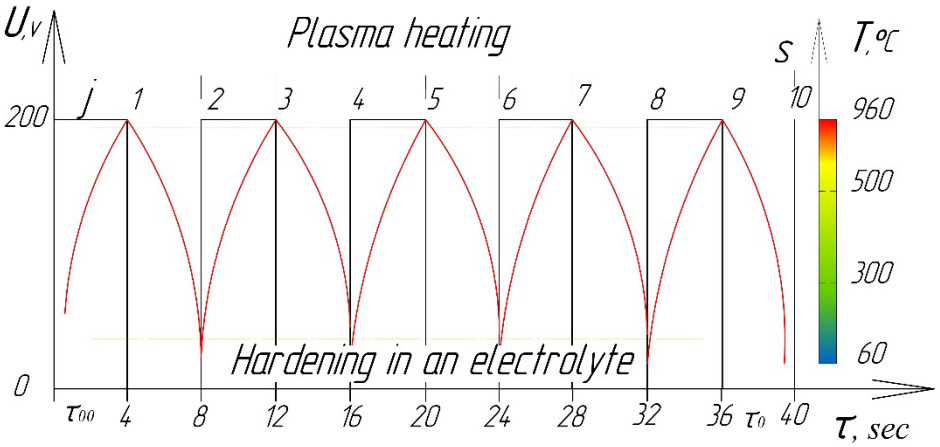

Fig. 5. Cyclic electrolytic-plasma hardening

It was experimentally determined that over time, approximately by the total s_j = 10 cycle, τ=40th second, maximum heating from the plasma temperature and hardening occur over the entire cross-section of the cone tip due to the above factors [20].

To verify the constructed analytical model, an experiment was conducted to compare the thermal impact on the tip surface microstructure and wear resistance. A comparison was made with the results of numerical simulation by the finite element method and experimental data on increasing the wear resistance of the working surface of the tip after EPH [21].

The microstructure of steel 14X17H2 (431 AISI, SAE, ASTM) in the initial state is a coarse-grained martensitic-ferritic structure, Figure 6a. The lightest areas are δ-ferrite, and the somewhat darker areas are martensite, which in this case are not sufficiently etched. In the microstructure of δ-ferrite, the presence of finely dispersed alloying elements Cr and Ni improves manufacturability during deformation and quenching cooling, reducing the level of temporary and residual stresses due to their relaxation during section deformation of the plastic phase (δ-ferrite) [22].

In the microstructure of steel 14X17H2 (431 AISI, SAE, ASTM), after the above-described EPH, the formation of a fine-grained microstructure is observed, as well as the formation of carbides in the body of the grain and at the boundaries of the austenite grains, Figure 6b. During cyclic electrolytic plasma heating to temperatures of 910-960°C and quenching in an electrolyte flow at 330-360°C, the steel structure is a combination of light - strongly etched and dark areas. Dark areas are martensite, and light areas are δ-ferrite. Ferrite sections are divided into separate grains, and the boundaries between ferrite-martensite grains are decorated with a carbide mesh.

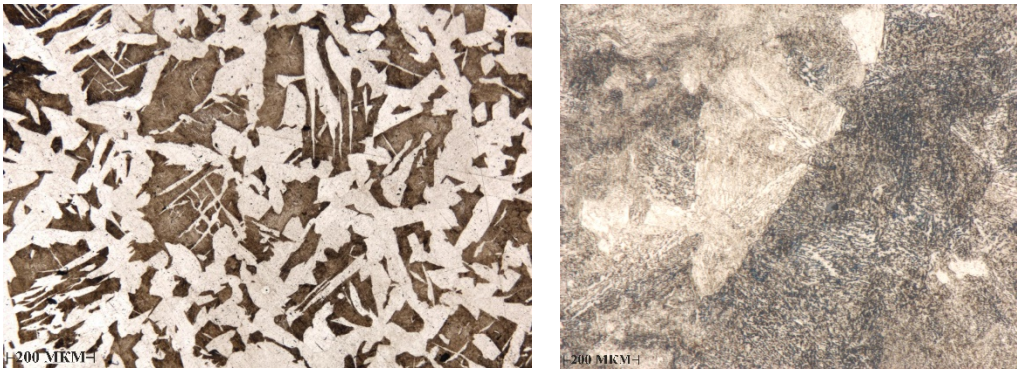

a) in an initial state b) after quenching EPH

Fig. 6. Steel microstructure 14X17H2 (431 AISI, SAE, ASTM)

This is due to the fact that at a temperature of 870 °C, steel is in the range of triple equilibrium α → γ → k, in contrast to t = 1050 °C, where the equilibrium is double γ + α [23]. Phase transformations of steel 14X17H2 (431 AISI, SAE, ASTM) are temper sorbitol and δ-ferrite, Figure 6b. The amount of δ-ferrite exceeds by 15–20% its amount after quenching from a temperature of 960°C. In this case, there are no quenching cracks in the samples.

When studying the modes of EPH hardening for the tendency to intergranular corrosion - MCC steel 14X17N2 (431 AISI, SAE, ASTM), much attention was paid to the possibility of reducing the grain size of ferrite and martensite and discontinuity of ferrite chains, since it is known that the main proportion of carbides in steel 14X17N2 (431 AISI, SAE, ASTM) stands out at the ferrite-martensite and ferrite-ferrite interface [24]. After thermal EPH, resistance to intergranular corrosion is supposedly provided by saturation with carbon ions from the decomposition of 10% soda ash of the electrolyte during high-speed quenching.

The throttle tip on a conical mating pair "tip-seat" provides tightness of high-pressure oil products. Therefore, the high hardness of the conical surface, with a damping core, is a very important indicator. The microhardness was measured, respectively, from the sample in the initial state and after electrolytic-plasma hardening. The measurement results, Figure 7, indicate that after electrolytic plasma hardening, the microhardness more than doubled: on average, from HV 231 to HV 640 kgf/mm2.

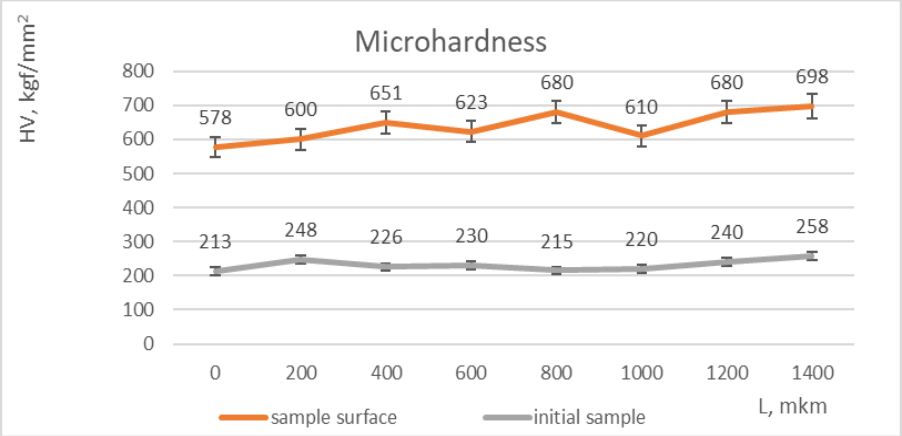

Fig. 7. The value of the microhardness of steel 14X17H2 (431 AISI, SAE, ASTM)

When converting the hardness, the average value of the hardness of the hardened surface of the tip by the method of electrolytic plasma hardening corresponds to 54–60 HRC, which significantly exceeds the hardness of 255–260 HB of steel in the as-delivered condition [25].

The tip wear mechanism during throttle operation is complex and includes abrasive, adhesive, and diffusion wear. In this regard, the tribological properties of the samples in the initial states and after the EPH were studied. The test conditions are chosen close to the operating conditions of high-pressure shut-off valves. Tribological properties were determined from the results of a series of tests [26].

The experimental curves of the dependence of the coefficient of friction on the sliding distance of the original sample are shown in Figure 8. The values of the coefficient of dry friction at the beginning of the test increase from 0.05 to an average of 0.45, which roughly corresponds to rubbing materials "steel-steel" during sliding.

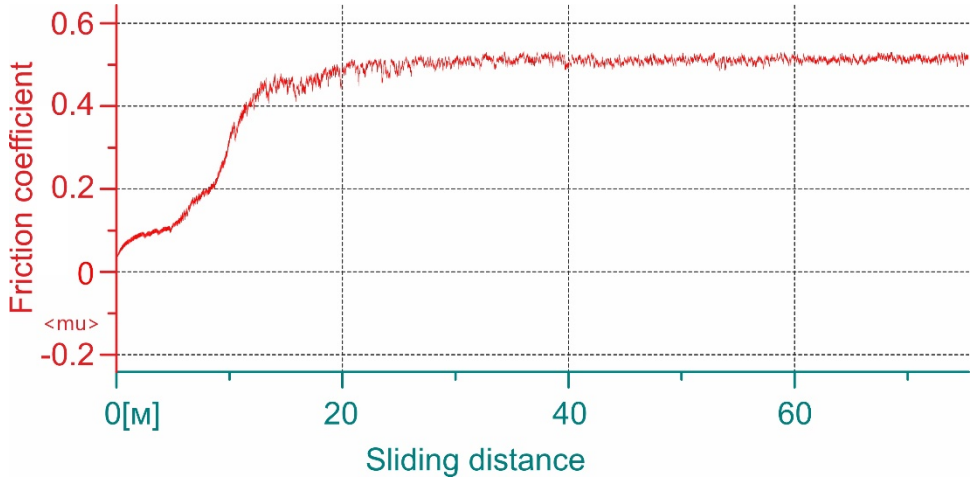

Fig. 8. Test protocol for friction and wear of steel 14X17H2 (431 AISI, SAE, ASTM) in the initial states

Figure 9 shows the coefficient of friction of samples of steel 14X17N2 (431 AISI, SAE, ASTM) after EPH during cyclic electrolyte-plasma heating to temperatures of 910–960°C and quenching in an electrolyte flow at 330–360°C, decreases on average from 0.45 to 0.25 and remains at this level until the end of friction [27].

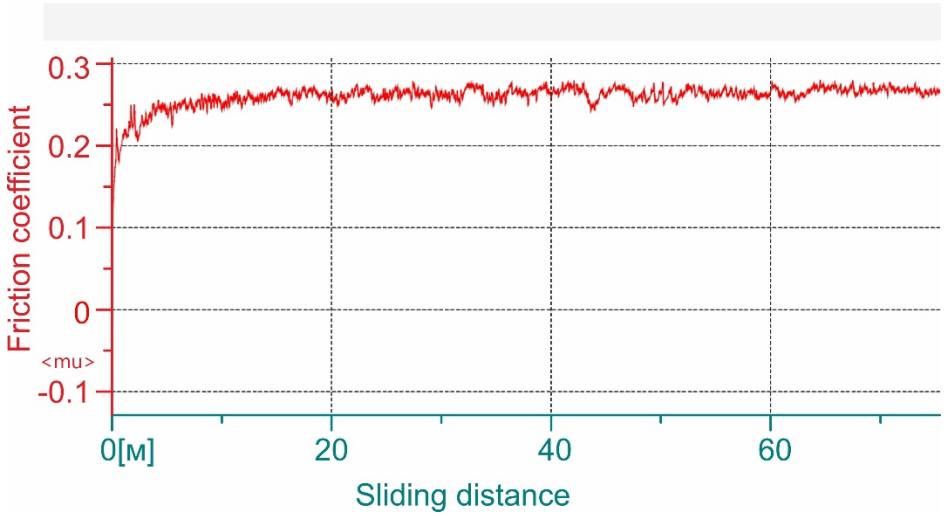

Fig. 9. Test protocol for friction and wear of steel 14X17H2 (431 AISI, SAE, ASTM) about EPH

According to the results of a comparative analysis of the tribological properties (Figure 9), the EPH of steel 14X17H2 (431 AISI, SAE, ASTM) causes a significant 2.36 times to decrease in wear intensity without lubrication, under conditions of adhesive wear in the absence of noticeable frictional heating, as well as during sliding friction on a steel plate in the presence of lubricant, under conditions of boundary friction [28-29].

The tribological characteristics of the samples in the initial states and after the EPH were characterized by the wear intensity and friction coefficient, Table 2. After the EPH of the samples, an increase in wear resistance is observed under friction conditions without lubrication and with lubrication in water.

Table 2. Tribological properties of steel 14X17H2(431 AISI, SAE, ASTM)

№	Sample condition	Tribological properties			
		lubricated friction		friction without lubrication	
		Ih, $mm^3/(N*m)$	f	Ih, $mm^3/(N*m)$	f
1	Initial	$2,74\times10^{-6}$	0,11	$4,83\times10^{-4}$	0,45
2	After EPH	$1,07\times10^{-6}$	0,07	$2,04\times10^{-4}$	0,25

Under conditions of sliding friction with lubrication on a plate made of austenitic stainless steel 12X18N10T (321S31) [30-31], for the initial structural states of steel 14X17N2 (431 AISI, SAE, ASTM), a decrease in wear intensity by 2.56 times after EPH was found, Table 2.

Thus, the results of studies of the electrolytic-plasma hardening of the tip indicate an increase in the hardness and wear resistance of the tip and a significant reduction in the hardening time of the working surface from 20 hours to 40 seconds of cyclic hardening. High-speed electrolytic-plasma hardening of steel 14Kh17N2 (431 AISI, SAE, ASTM) significantly reduces labor intensity, and energy consumption and lends itself well to process automation [32-34].

The article is financially supported by the "Science Committee of the Ministry of Education and Science of the Republic of Kazakhstan" within the framework of the grant project IRN AR09058518 "Increasing the wear resistance of materials in the engineering industry by electrolyte-plasma modification".

4 CONCLUSION

1. Analytical and experimental studies have determined the optimal temperature for electrolytic-plasma heating of a tip made of steel 14X17H2 (431 AISI, SAE, ASTM) to 910-960°C and quenching in an electrolyte flow at 330-360 °C.

   Mathematically calculated modes of cyclic electrolyte-plasma hardening of the tip. The hardening temperature of the tip from the electrolyte plasma Theat=930-960°C, Q1=500 J is reached at the time τ1 = τ00= 4 s. The hardening time in the electrolyte flow Tzak=330-360°C is equal to τ2=τ00+τ1=8 s. Experimentally determined the total number of cycles sj=10 and at τ=40th second there is maximum heating from the plasma temperature and hardening over the entire cross-section of the cone tip. Under these conditions, structural-phase transformations occur that strengthen the steel of the tip.
2. Structural-phase transformations of steel 14X17N2 (431 AISI, SAE, ASTM) after cyclic EPH are tempering sorbate and δ-ferrite. This provides resistance to intergranular corrosion, which is supposedly carried out by saturation with carbon ions from the decomposition of 10% soda ash of the electrolyte and high-speed hardening.

3. The value of microhardness indicates an increase from the initial state, on average, HV 231 to HV 640 kgf/mm2, more than two times after electrolytic-plasma hardening
4. The tribological characteristics of the samples in the initial state and after EPH were characterized by the intensity of wear on the working surface of the tip. After EPH, an increase in the wear resistance of samples under dry friction conditions is observed. According to the results of a comparative analysis of tribological properties, electrolytic-plasma hardening of steel 14X17H2 (431 AISI, SAE, ASTM) causes a decrease in wear rate by 2.36 times, without lubrication. Under conditions of sliding friction with lubrication on a plate made of austenitic stainless steel 12X18H10T (321S31) relative to the initial structural states of steel 14X17H2 (431 AISI, SAE, ASTM), a decrease in wear intensity by 2.56 times after EPH was established.

5 REFERENCES

[1] Kombayev, K., Muzdybayev, M., Muzdybayeva, A., Myrzabekova, D., Wieleba, W., & Leśniewski, T. (2022). Functional Surface Layer Strengthening and Wear Resistance Increasing of a Low Carbon Steel by Electrolytic-Plasma Processing. Strojniški vestnik-Journal of Mechanical Engineering, vol. 68(9), 542-551.

[2] ASTM E1558-09(2014), Standard Guide for Electrolytic Polishing of Metallographic Specimens, ASTM International, West Conshohocken, PA, 2014, www.astm.org

[3] Smyrnova, K., Sahul, M., Haršáni, M., Pogrebnjak, A., Ivashchenko, V., Beresnev, V., Vanco, L. (2022). Microstructure, Mechanical and Tribological Properties of Advanced Layered WN/MeN (Me= Zr, Cr, Mo, Nb) Nanocomposite Coatings. Nanomaterials, vol. 12, 395.

[4] Pogrebnjak, A. D., Beresnev, V. M., Bondar, O. V., Postolnyi, B. O., Zaleski, K., Coy, E., & Araujo, J. P. (2018). Superhard CrN/MoN coatings with multilayer architecture. Materials & Design, vol. 153, 47-59.

[5] Doudkin, M., Kombayev, K., Kim, A., Azamatov, B., Azamatova, Zh. (2020). Research of cutting temperature reducing of titanium alloy grade 5 below polymorphic transformation depending on calculation of cutting modes. International Journal of Mechanical and Production Engineering Research and Development (IJMPERD), vol. 10, issue 2, 747–758, https://doi.org/10.24247/ijmperdapr202074.

[6] Mikhalev, A. D., Dyadyura, K. A., Lebedynskyi, I., Bratushka, S. N., & Kravchenko, Y. O. (2019). Structure, morphology, and elemental-phase composition of j02002 steel as a result of electrolytic-plasma processing. High Temperature Material Processes: An International Quarterly of High-Technology Plasma Processes, 23(1).

[7] Kombayev, K. K., Doudkin, M. V., Kim, A. I., Mlynczak, M., Rakhadilov, B.K. (2019). Surface hardening of the aluminum alloys Al3 by electrolytic-plasma treatment. News Of the national academy of sciences of the republic of Kazakhstan. Series of geology and technical sciences, vol. 4, no. 436, 222 – 229, https://doi.org/10.32014/2019.2518-170X.117.

[8] García-Leóna, R.A., Martínez-Trinidada, J., Campos-Silvaa, I., Figueroa-López U., Guevara-Morales B., A. (2021). Development of tribological maps on borided AISI 316L stainless steel under ball-on-flat wet sliding conditions. Tribology International, vol. 163, 107161, https://doi.org/10.1016/j.triboint.2021.107161.

[9] García-Leóna, R.A., Martínez-Trinidada, J., Zepeda-Bautistaa, R., Campos-Silvaa, I., Guevara-Morales B, A., Martínez-Londoñoa, J., Barbosa-Saldaña, J. (2021). Dry sliding wear test on borided AISI 316L stainless steel under ball-on-flat configuration: A statistical analysis. Tribology International, 157, 106885, https://doi.org/10.1016/j.triboint.2021.106885.

[10] Korzhyk, V., Tyurin, Yu., Kolisnichenko, O. (2021). Surface modification of metal products by electrolyte plasma. Kharkiv: PC TECHNOLOGY CENTER 180.

[11] Kozha, E., Smagulov, D.U., Akhmetova, G.E., Kombaev, K.K. (2017). Laboratory installation for electrolytic-plasma treatment of steel. NEWS of national academy of sciences of the republic of Kazakhstan, vol. 4(424), 219-225.

[12] Steblyanko, V. L., & Ponomarev, A. P. (2016). Plasma-Electrolytic Treatment as an Innovative and Resource-Saving Technology of Metal Surface Treatment. In Materials Science Forum, vol. 870, 416-421.

[13] Kombayev, K., Kim, A., Yelemanov, D., Sypainova, G. (2022). Strengthening of Low-Carbon Alloy Steel by Electrolytic-Plasma Hardening. International Review of Mechanical Engineering (I.RE.M.E.), vol. 16(2), 84–91. DOI: 10.15866/ireme.v16i2.21712

[14] Popov, A. I., Radkevich, M. M., & Teplukhin, V. G. (2020). Thinnest finishing treatment with a focused jet of electrolytic plasma. In Advances in Mechanical Engineering, 139-149.

[15] Ayday, A., Derya, K., Şükran Demirkıran, A. (2022). The Effects of overlapping in electrolytic plasma hardening on wear behavior of carbon steel. Transactions of the Indian Institute of Metals, vol. 75.1, 27-33.

[16] Liang, J., Hossain, N. I., Wahab, M. A., & Guo, S. (2012). Improvement of Corrosion Resistance on a Low Carbon Steel 1018 in 3.5% NaCl Solution by Electrolytic-Plasma-Process (EPP). In ASME International Mechanical Engineering Congress and Exposition, vol. 45196, 821-825.

[17] Dayanç, A., B. Karaca, and L. Kumruoğlu. (2017). The cathodic electrolytic plasma hardening of steel and cast iron based automotive camshafts. Acta Physica Polonica A, vol. 131.3, 374-378.

[18] Popova, N. A., et al. (2020). Structure and Phase Composition of Ferriticperlitic Steel Surface after Electrolytic Plasma Quenching. Russian Physics Journal, vol. 63.5, 791-796.

[19] Mikhalev, A. D., et al. (2019). Structure, morphology, and elemental-phase composition of j02002 steel as a result of electrolytic-plasma processing. High Temperature Material Processes: An International Quarterly of High-Technology Plasma Processes, vol. 23.1

[20] Miller, D. J., Dreyer, D. R., Bielawski, C. W., Paul, D. R., & Freeman, B. D. (2017). Surface modification of water purification membranes. Angewandte Chemie International Edition, vol. 56(17), 4662-4711.

[21] Zhang, F., et al. (2021). Effect of annealing temperature on microstructure and mechanical properties of plasma sprayed TiC-Ti5Si3-Ti3SiC2 composite coatings. Surface and Coatings Technology, vol. 422, 127581.

[22] Wieleba, W. (2005). The role of internal friction in the process of energy dissipation during PTFE composite sliding against steel. Wear, vol. 258(5-6), 870-876.

[23] Wieleba, W., (2007). The mechanism of tribological wear of thermoplastic materials. Archives of Civil and Mechanical Engineering, vol. 7(4), 185-199.

[24] Rakhadilov, B. K., Buranich, V. V., Satbayeva, Z. A., Sagdoldina, Z. B., Kozhanova, R. S., Pogrebnjak, A. D. (2020). The cathodic electrolytic plasma hardening of the 20Cr2Ni4A chromium-nickel steel. Journal of Materials Research and Technology, vol. 9(4), 6969-6976. doi:10.1016/j.jmrt.2020.05.020.

[25] Mazhyn, S., Bauyrzhan, R., Erlan, B., Michael, S. (2014). Change of structure and mechanical properties of R6M5 steel surface layer at electrolytic-plasma nitriding doi:10.4028/www.scientific.net/AMR.1040.753

[26] Rakhadilov, B., Zhurerova, L., Pavlov, A. (2016). Method of electrolyte-plasma surface hardening of 65G and 20GL low-alloy steels samples. IOP Conference Series: Materials Science and Engineering, vol. 142(1) doi:10.1088/1757-899X/142/1/012028.

[27] Rakhadilov, B. K., Kenesbekov, A. B., Sagdoldina, Z. B., Stepanova, O. A. (2020). Tribological And Corrosion Characteristics Of Coatings Based On Chromium Nitride Deposited By The Mechanochemical Method. Journal of Physics: Conference Series, vol. 1529, no. 4, 042101.

[28] Kengesbekov, A., Rakhadilov, B., Sagdoldina, Z., Buitkenov, D., Dosymov, Y., Kylyshkanov, M. (2022). Improving the Efficiency of Air Plasma Spraying of Titanium Nitride Powder. Coatings, vol. 12(11), 1644.

[29] Ptak, A., Taciak, P. and Wieleba, W., (2021). Effect of Temperature on the Tribological Properties of Selected Thermoplastic Materials Cooperating with Aluminium Alloy. Materials, vol. 14(23), 7318.

[30] Pawlak, W., Wieleba, W. and Wróblewski, R. (2019). Research of tribological properties of polylactide (PLA) in the 3D printing process in comparison to the injection process. Tribologia.

[31] Doudkin, M., Kim, A., Sakimov, M. (2019). Mathematical and experimental study of deformations of a steel roll of a road roller with a variable geometry of a contact surface. Production Engineering Archives, vol. 25, 1-7. https://doi.org/10.30657/pea.2019.25.01

[32] Doudkin, M., Kim, A., Młyńczak, M., Kustarev, G., Kim, V. (2019). Development and parameter justification of vibroscreen feed elements. Mining Machines and Earth-Moving Equipment: Problems of Design, Research and Maintenance, 203–226.

[33] Doudkin, M., Kim, A., Savelyev, A., Zhileikin, A., Gribb, V., Mikhailovskaya, V. (2020). Modernization of the Metal Structure of the Grader Working Equipment. International Review of Mechanical Engineering (I.RE.M.E.), vol. 14, no. 1, 1-8

[34] Vavilov, A., Kim, A., Guryanov, G., Likunov, A. (2020). New technology of the steel fiber manufacturing from technogenic waste. International Journal of Mechanical and Production Engineering Research and Development, vol. 10(3), 611–622.

Paper submitted: 18.01.2023.

Paper accepted: 01.06.2023.